

BOUNDARY LAYER SEPARATION CONTROL ON AIRFOILS AND WINGS WITH FINITE TRIPS AT LOW REYNOLDS NUMBERS

Nianhua Liu and Serhiy Yarusevych†
Mechanical and Mechatronics Engineering
University of Waterloo
200 University Ave W, Waterloo, ON, Canada
†syarus@uwaterloo.ca

ABSTRACT

The effect of boundary layer trip segments on the aerodynamic performance and flow development over the airfoil and finite wing with a NACA 0018 profile is investigated experimentally at angle of attack of $\alpha = 5^\circ$ and chord Reynolds number of $Re_c = 60,000$. Under the selected conditions, both the airfoil and wing models are stalled. Direct force measurement and particle image velocimetry (PIV) measurement are carried out to characterize the effects of boundary layer trips with different spanwise lengths. The results demonstrate that a substantial aerodynamic gain can be achieved when boundary layer trips are centered at the midspan of the models, while the trip spanwise length does not affect the gains significantly for the range of trip segment geometries investigated. The flow measurements show that trip segments affect the spanwise region whose extent exceeds substantially the spanwise length of the trip. The trip segment induces transition downstream, and induces the formation of two three-dimensional laminar separation bubbles on either side of the segment. The associated changes to shear layer dynamics are explored and demonstrate changes to shear layer shedding characteristics.

INTRODUCTION

Lifting surfaces are prone to suction surface boundary layer separation, especially under aerodynamically low chord Reynolds number conditions, $Re < 500,000$ (Carmichael, 1981), when the boundary layer remains laminar upstream of separation. When separation takes place, it typically brings about a decrease in lift-to-drag ratio (Mueller & DeLaurier, 2003), and the associated flow unsteadiness can lead to structural vibrations and noise.

Mean separated shear layer reattachment might occur due to laminar-turbulent transition. Under sufficiently high Reynolds numbers, the separated shear layer undergoes transition, enhancing momentum exchange that enables flow reattachment to the suction surface in the mean sense (Lissaman, 1983). The near-wall flow region bound by the separation and reattachment locations is commonly referred to as Laminar Separation Bubble (LSB). Such a flow configuration is associated with milder degradation of performance compared to stall (Jones, 1934).

Boundary layer tripping is commonly employed to induce an earlier transition to turbulence and prevent laminar boundary layer separation. Various boundary layer trips have been investigated, including trip wires (Huber & Mueller, 1987), rectangular bar trips (Volino, 2003) and zigzag trips (Elsinga &

Westerweel, 2012). Two-dimensional trips, such as trip wires and bar trips, enhance the growth of Tollmien-Schlichting waves (Zhang *et al.*, 2023). In contrast, three-dimensional trips, such as zigzag trips and roughness element trips, induce three-dimensional flow structures that accelerate transition (Elsinga & Westerweel, 2012; Zhang *et al.*, 2023). Boundary layer tripping by roughness elements was the focus of several studies, and general trip design guidelines have been proposed (e.g., Braslow *et al.* (1966), Elsinga & Westerweel (2012), Smith & Clutter (1959), Braslow & Knox (1958)).

The effects of boundary layer tripping on the aerodynamic performance of airfoils at low Reynolds numbers have also been considered in previous investigations. Lyon *et al.* (1997) proposed that boundary layer tripping can reduce drag, especially when long separation bubbles occur in the baseline flow. Drag reduction was also reported by Boermans *et al.* (1989) and Huber & Mueller (1987), who applied a zigzag trip and trip wire, respectively. Boermans *et al.* (1989) achieved an increase in the maximum lift coefficient using vortex generators. Huber & Mueller (1987) found that, with appropriate positioning, a trip wire can increase the maximum lift-to-drag ratio and avert hysteresis. In contrast, Bloch & Mueller (1986) observed that the distributed roughness elements added near the suction peak induced earlier stall. Selig & McGranahan (2004) found that adding zigzag trips on both sides of the airfoil models can either be aerodynamically beneficial or detrimental, depending on the presence and size of LSBs.

The objective of this study is to investigate the effect of a finite trip segment on the flow development and aerodynamic performance of an airfoil and wing. It will be shown that a trip segment can affect the flow over a portion of the lifting surface significantly larger than the spanwise extent of the trip, inducing significant changes to performance metrics.

METHODOLOGY

All experiments were conducted in the recirculating wind tunnel at the University of Waterloo. The test section of this facility has a square cross-section of $0.61m \times 0.61m$ and a length of $2.4m$. The freestream velocity within the test section was calibrated based on the pressure drop along the upstream 9:1 contraction.

The wing model, with a NACA 0018 profile, had a chord of $c = 0.2m$ and an aspect ratio of $L/c = 2.5$. With a half-chord length extension attached to the wing tip, as indicated in Figure 1, the model spans the test section, forming the airfoil model.

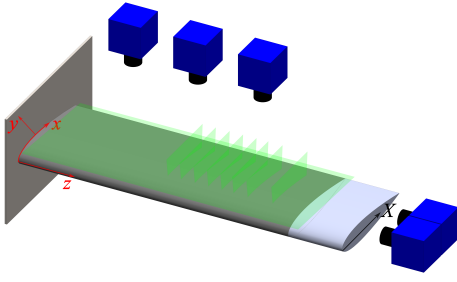


Figure 1. Experimental setup for PIV measurements and the coordinate systems for data presentation. Green surfaces are PIV measurement planes.

All experiments were conducted at a geometric angle of attack of $\alpha = 5^\circ$ and a chord-based Reynolds number of $Re_c = 60,000$, producing stalled conditions. Separation control was conducted by attaching boundary layer trips on the suction side of the models. The boundary layer trips were made of randomly distributed sand roughness elements, with a diameter within 0.85% to 1% of the chord, placed on a double side tape with a thickness of around 0.065% of the chord. The streamwise dimension of trips was $0.06c$, and the trailing edge of boundary layer trips was $0.2c$ downstream from the model leading edge. The effects of spanwise trip length (l) were considered over a range of trip length ratios (l/L) from 0.08 to 1, with trips centred at the midspan plane of the models. Moreover, the impact of spanwise trip location on the aerodynamic performance of both airfoil and wing models was investigated by placing a boundary layer trip segment at different spanwise locations, with $l/L = 0.08$ for airfoil and $l/L = 0.10$ for wing.

Direct aerodynamic force measurements were facilitated by a six-component force balance. Flow field characterisation was performed using two-component Particle Image Velocimetry (PIV), obtaining both non-time-resolved and time-resolved snapshots. Non-time-resolved PIV measurements were conducted from top and side views of the models, with three and two LaVision Imager sCMOS 5.5 megapixel cameras arranged in a side-by-side manner, respectively (Figure 1). For top view measurements, the measurement plane was set parallel to the model chord, at a minimum height of $0.02c$ from the model surface. Side view measurements involved eight measurement planes in total, within a spanwise range of $1.5 < z/c < 2.25$. Time-resolved measurements were carried out from the side view, with two Photron SA4 cameras arranged in the same manner as shown in Figure 1. For all PIV configurations, the flow was seeded using water-glycol fog particles of around 1 micron in diameter, which were illuminated by a Photonics DM20-527 Nd:YLF pulsed laser. Dual-frame images were acquired at sampling frequencies of 25 Hz and 2500 Hz to obtain non-time-resolved and time-resolved data, respectively. A surface-attached coordinate system is used for presenting side-view PIV results, as defined in Figure 1. A chord-based coordinate system is used for the top-view results, with the X axis parallel to the chord.

RESULTS

The effects of boundary layer trip length on the aerodynamic performance of both airfoil and wing are quantified in Figure 2. The results show substantial gains in lift coefficients produced with boundary layer trips, especially on the airfoil model. Moreover, considerable improvements in aerodynamic

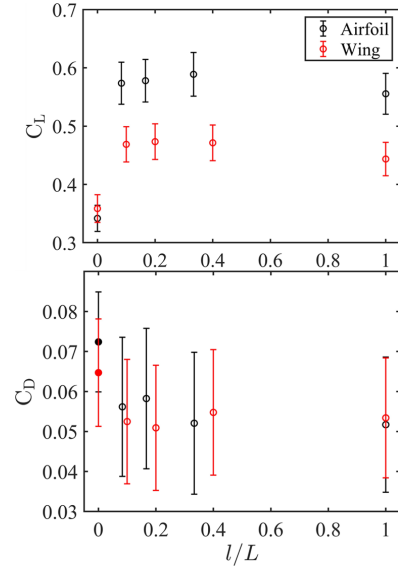


Figure 2. The effect of boundary layer trip length on lift and drag coefficients. l : spanwise length of the trip. L : Model span. Error bars show the uncertainty with 95% confidence.

performance are achieved over a wide range of boundary layer trip length ratios, with results comparable to those achieved with a trip extending over the entire model span ($l/L = 1$). The trip segments also produce a notable and repeatable decrease in drag coefficient, although the change is within the measurement uncertainty.

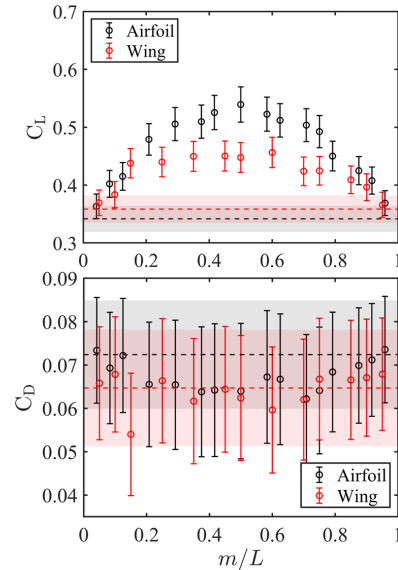


Figure 3. The effect of trip spanwise location on lift and drag coefficients. L : Model span. m : distance from the trip midspan to the model base. Error bars illustrate measurement uncertainty with 95% confidence. A boundary layer trip with $l/L = 8\%$ (Airfoil) and 10% (Wing) was applied. Black (airfoil) and red (wing) dashed lines show the lift and drag coefficients without flow control, with shadowed regions illustrating uncertainty bounds.

Figure 3 depicts the effect of boundary layer trip spanwise location on the aerodynamic performance of both airfoil

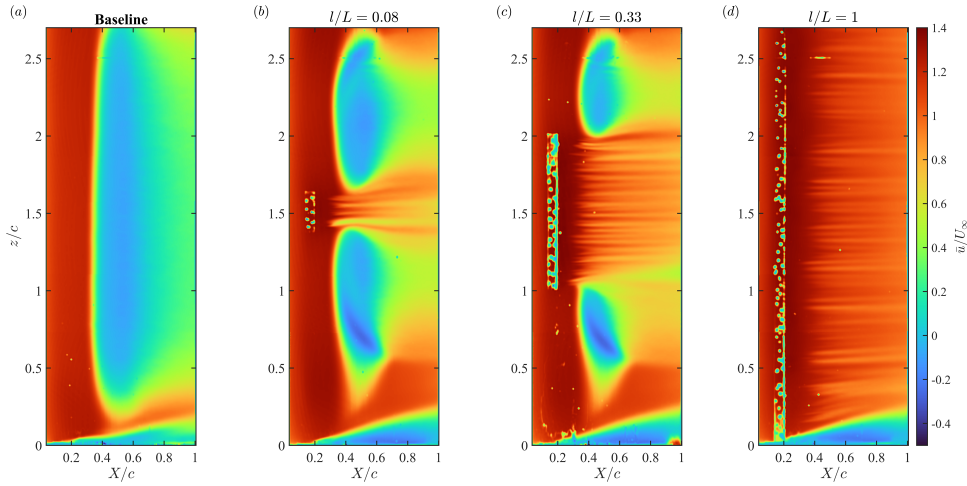


Figure 4. The effect of boundary layer trip on the mean flow topology (Top view of airfoil). l : spanwise length of the trip. L : model span.

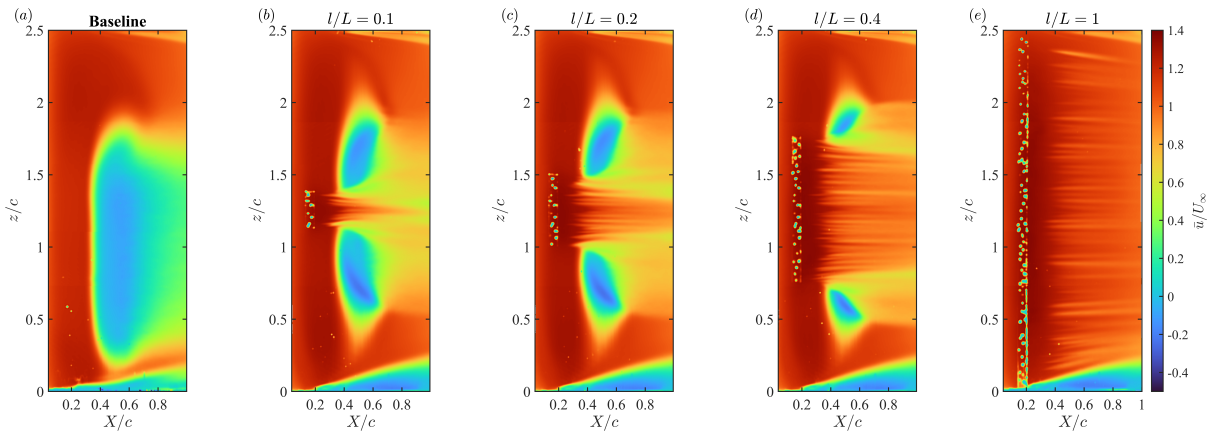


Figure 5. The effect of boundary layer trip on the mean flow topology (Top view of wing). l : spanwise length of the trip. L : model span.

and wing models using $l/L = 0.08$ and $l/L = 0.10$ trips, respectively. For both models, the maximum performance gains are achieved with the trip segment placed near the mid-span, which decrease progressively when trips are placed closer to the root/tip region. In the subsequent analysis, the results will be presented only for the trips centred at the midspan of the models.

To shed light on the underlying changes in the flow development, Figures 4 and 5 present a comparison of top-view mean streamwise velocity fields for the airfoil and wing models, respectively. The corresponding side-view results at selected spanwise planes are presented in Figures 6 and 7. For the side-view PIV results, the separated flow region is identified by a dividing streamline (black line), as defined by Horton (1968).

A typical stalled flow development is seen for the baseline case on the airfoil (Figure 4a and 6a) and wing (Figure 5a). Adding the trip changes significantly the flow over the suction side of both airfoil and wing; however, unlike the resultant effect on the lift, the changes in the flow development vary notably with the trip length ratio.

When a trip is added across the entire span of the models, the large separated flow region is eliminated, as expected (Figures 4d and 5e). The results show that adding a trip segment at the midspan leads to the same effect immediately downstream of the trip (Figure 4b – c and 5b – d). Further, this splits the

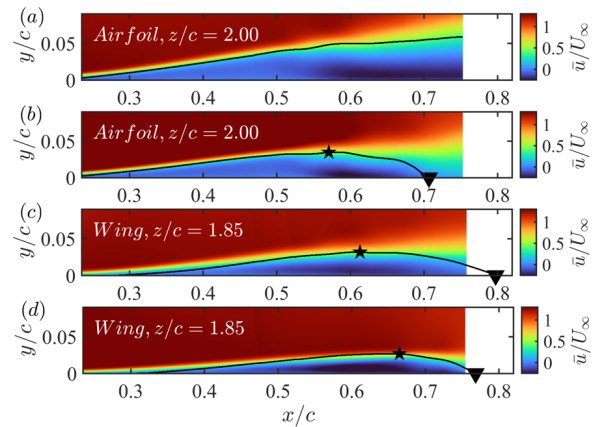


Figure 6. The effect of boundary layer trip segment on the mean streamwise velocity field. (a) and (c) show baseline cases with no flow control, (b) and (d) have a boundary layer trip segment, $l/L = 0.08$ and 0.10 for airfoil and wing respectively, centered the model midspan. Black solid curves are dividing streamlines. The asterisk and triangle mark the highest point of the dividing streamline and the mean reattachment location, respectively.

separated flow region into two parts, with the extent of each diminishing with increasing the trip length ratio.

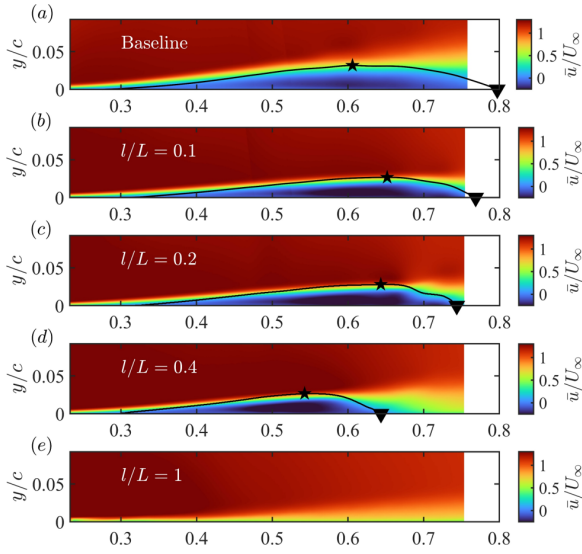


Figure 7. The effect of trip length on the mean streamwise velocity for the wing model. Black solid curves are dividing streamlines, while the asterisk and triangle mark the highest point of the dividing streamline and the estimated mean reattachment location, respectively. l : spanwise length of the trip. L : wing span.

The side-view results in Figures 6 and 7 show that the baseline flow on the airfoil separates without a subsequent reattachment in Figure 6a. Adding a trip spanning $1.38 < z/c < 1.63$ induces mean flow reattachment at $z/c = 2.00$ (Figure 6b). It can be deduced that the addition of a finite trip leads to the formation of two three-dimensional LSBs separated by a region of turbulent flow immediately downstream of the trip. The induced changes to the flow topology are responsible for the performance gains produced by the addition of trip segments, as seen in Figure 2.

It should be noted that, for the wing model, the wing tip effects eliminate the separated flow region in the immediate proximity of the tip (Figure 5a) and induce flow reattachment farther inboard (Figure 6c). Here, the addition of the trip segment at mid-span is seen to reduce the streamwise extent of the separated flow at the same plane close to the wing tip (Figure 6d).

Figure 7 provides insight into the effect of trip length on the mean flow topology at the measurement plane $z/c = 1.85$ on the wing. The results show that increasing the trip length ratio leads to the shortening of the separated flow region away from the trip. Confirming qualitative observations that can be made from top-view measurements (Figure 5), the side-view data presented in Figure 6 show that the reattachment location is moving upstream with increasing the trip segment length ratio, leading to the overall decrease in the length of the separation bubble.

The RMS fluctuating velocity fields in Figure 8 depict notable changes induced by the addition of finite trip segments outside their bounds for the airfoil. For all the cases presented, the most significant streamwise and wall-normal velocity fluctuations occur close to the displacement thickness (black dashed curves). For the baseline flow, significant

streamwise velocity fluctuations are seen in the core of the shear layer in the entire field of view (Figure 8a), while vertical velocity fluctuations become substantial farther downstream (Figure 8c). This points to shear layer flapping (Burgmann & Schröder, 2008; Simoni *et al.*, 2012), which is diminished notably when the addition of a trip segment induces flow reattachment (Figures 8b and d). With the trip segment applied, the maximum magnitude of streamwise velocity fluctuations diminishes, while higher wall-normal fluctuations are attained. This is also accompanied by the decrease in the upstream extent of significant velocity fluctuations, indicating less pronounced shear layer flapping and stronger shear layer roll-up.

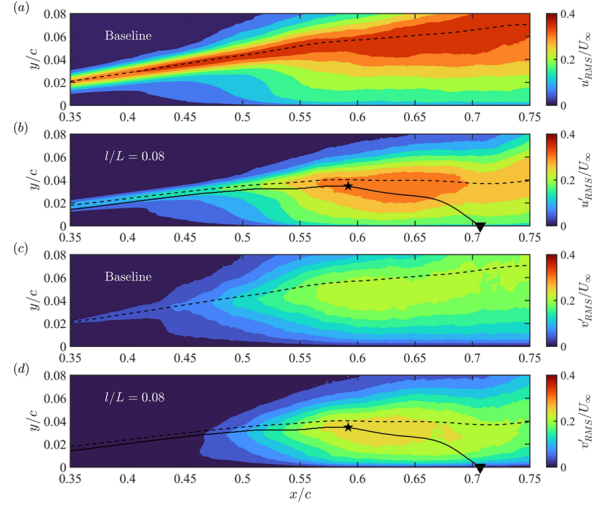


Figure 8. The effect of trip segment on u'_{RMS} and v'_{RMS} fields at $z/c = 2.00$ on the airfoil.

The underlying flow dynamics is explored in Figure 9, which shows a series of instantaneous λ_2 contours to aid vortex identification. These time-resolved results show a formation of shear layer roll-up vortices for the baseline (Figure 9a) and tripped (Figure 9b) flow cases. The cores of individual structures are tracked by red dashed lines. The formation of shear layer vortices coincides with the region of significant wall-normal velocity fluctuations in Figure 8. As the addition of the trip segment induces flow reattachment, the vortices are formed closer to the surface at this measurement plane. However, the characteristic streamwise lengthscale does not change significantly, with $\lambda_x/c \approx 0.055$ for both cases. In contrast, the streamwise vortex advection speed increases by more than 30% for the tripped case, pointing to the increase in shedding frequency.

Figure 10 demonstrates the effect of boundary layer tripping on the shear layer shedding frequency at a spanwise plane away from the trip. The results show power spectral density contours from wall-normal velocity fluctuations sampled along the displacement thickness. The results show amplification of fluctuations in a relatively narrow frequency band centred at $fc/U_\infty = 7.20$ for the baseline case. When the trip segment is added, perturbations are amplified over a slightly broader frequency range. At a streamwise location of $x/c = 0.5$, where prominent vortex shedding can be seen for the cases presented, the dominant spectral energy content is centred at $fc/U_\infty = 7.63$ for the baseline flow (Figure 10a), and at $fc/U_\infty = 9.53$ when the trip segment is applied (Figure 10b). This confirms the earlier deduction that the average

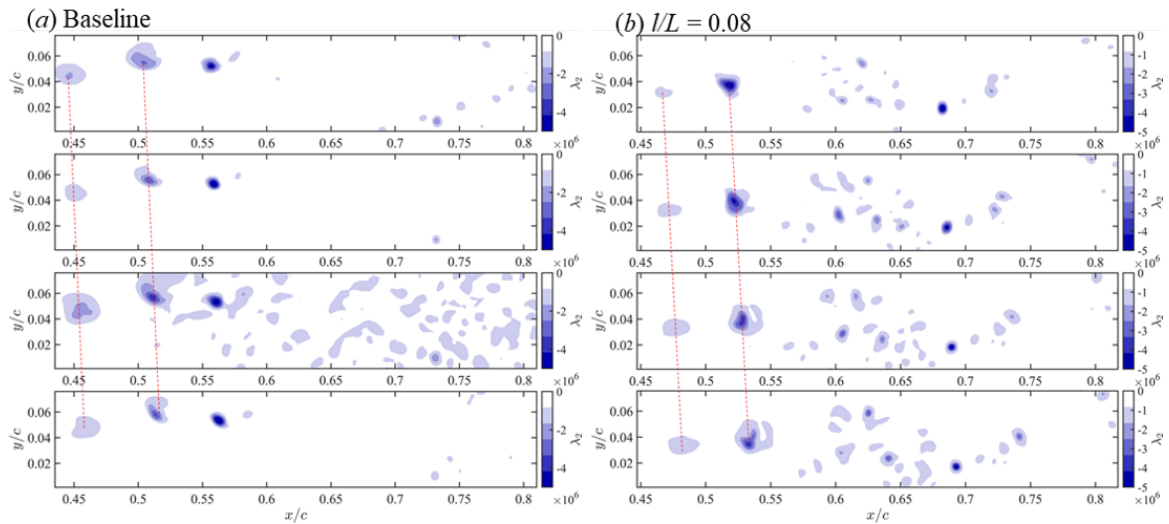


Figure 9. Sequences of instantaneous λ_2 contour showing the effect of boundary layer trip segment on vortex dynamics on the airfoil. The trip segment in (b) is centered the midspan of the airfoil ($z/c = 1.50$). Measurement planes: (a) $z/c = 1.50$, (b) $z/c = 2.00$.

shedding frequency increases when the trip segment induces flow reattachment and the formation of a three-dimensional LSB.

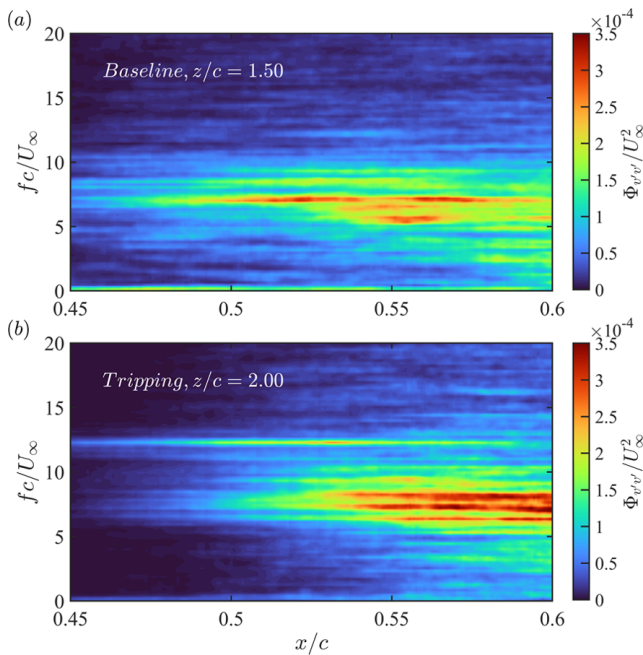


Figure 10. The effect of boundary layer trip segment ($l/L = 0.08$) on spectra of wall-normal velocity fluctuations sampled along the displacement thickness line on the airfoil.

CONCLUSION

In this paper, the effect of boundary layer trip segments on the aerodynamic performance and flow development over both airfoil and finite wing with a NACA 0018 profile is presented. A stalled baseline flow is considered at a geometric angle of attack of $\alpha = 5^\circ$ and a chord Reynolds number of $Re_c = 60,000$. The effect of boundary layer trips made of

randomly distributed sand roughness is considered for trips with spanwise length ranging from 8% to 100% of the model span. Direct force measurement and PIV measurement are performed to characterize the effect of trip segments on airfoil/wing performance and the associated flow development.

With a trip segment centered at the midspan of the models, substantial increases in lift coefficients can be produced by trip segments, with most significant gains obtained when trip segments are centred at the model midspan for both the airfoil and wing. Further, with midspan positioning, the effect of trip length ratio on the degree of performance improvement was not significant for the range of trip sizes considered here.

When placed at the model midspan, a boundary layer trip segment induces significant changes to the flow development over a spanwise region notably wider than the trip itself. The baseline stalled flow is divided into two regions with local reattachment in the mean sense, forming two three-dimensional LSBs. The induced reattachment is thus the main reason for the observed gain in lift. The spanwise extent of the two three-dimensional LSBs decreases with increasing the spanwise extent of the trip segment.

The results indicate that the shear layer flapping is diminished substantially once the addition of the trip induces flow reattachment. In contrast, the shear layer shedding in the formed LSBs appears to be intensified. While the characteristic spanwise wavelength of shear layer vortices does not change appreciably compared to the baseline flow, the average shedding frequency appears to increase on average.

REFERENCES

- Bloch, D. & Mueller, T. 1986 Effects of distributed grit roughness on separation and transition on an airfoil at low Reynolds numbers. In *4th Applied Aerodynamics Conference*, p. 1788.
- Boermans, L.M.M., Duyvis, F.J.D., Van Ingen, J.L. & Timmer, W.A. 1989 Experimental aerodynamic characteristics of the airfoils la 5055 and du 86-084/18 at low Reynolds numbers. In *Low Reynolds Number Aerodynamics: Proceedings of the Conference Notre Dame, Indiana, USA, 5–7 June 1989*, pp. 115–130. Springer.
- Braslow, A. L., Harris Jr, R.V. & Hicks, R. M. 1966 Use of grit-

- type boundary-layer transition trips on wind-tunnel models. *Tech. Rep.*.
- Braslow, A. L. & Knox, E. C. 1958 Simplified method for determination of critical height of distributed roughness particles for boundary-layer transition at mach numbers from 0 to 5. *Tech. Rep.*.
- Burgmann, S. & Schröder, W. 2008 Investigation of the vortex induced unsteadiness of a separation bubble via time-resolved and scanning piv measurements. *Experiments in fluids* **45** (4), 675–691.
- Carmichael, B.H. 1981 Low reynolds number airfoil survey, volume 1. *Tech. Rep.*.
- Elsinga, G.E. & Westerweel, J. 2012 Tomographic-piv measurement of the flow around a zigzag boundary layer trip. *Experiments in fluids* **52**, 865–876.
- Horton, H. P. 1968 Laminar separation bubbles in two and three dimensional incompressible flow .
- Huber, A.F. & Mueller, T.J. 1987 The effect of trip wire roughness on the performance of the wortmann fx 63-137 airfoil at low reynolds numbers. *Experiments in fluids* **5**, 263–272.
- Jones, B. M. 1934 Stalling. *The Aeronautical Journal* **38** (285), 753–770.
- Lissaman, P.B.S. 1983 Low-reynolds-number airfoils. *Annual review of fluid mechanics* **15** (1), 223–239.
- Lyon, C., Selig, M. & Broeren, A. 1997 Boundary layer trips on airfoils at low reynolds numbers. In *35th aerospace sciences meeting and exhibit*, p. 511.
- Mueller, T. J. & DeLaurier, J. D. 2003 Aerodynamics of small vehicles. *Annual review of fluid mechanics* **35** (1), 89–111.
- Selig, M. S & McGranahan, B. D. 2004 Wind tunnel aerodynamic tests of six airfoils for use on small wind turbines. *J. Sol. Energy Eng.* **126** (4), 986–1001.
- Simoni, D., Ubaldi, M. & Zunino, P. 2012 Loss production mechanisms in a laminar separation bubble. *Flow, turbulence and combustion* **89**, 547–562.
- Smith, A.M.O. & Clutter, D. W. 1959 The smallest height of roughness capable of affecting boundary-layer transition. *Journal of the Aerospace Sciences* **26** (4), 229–245.
- Volino, R. J. 2003 *Passive flow control on low-pressure turbine airfoils*, , vol. 36886.
- Zhang, J., Zhang, J., Fohlmeister, L.s & Scholz, P. 2023 Large-eddy simulation of boundary-layer transition over a zigzag trip. *AIAA Journal* **61** (3), 1032–1047.